Supporting Information

Improved Buried Interface Contact in Inverted Perovskite Solar Cells with Dual-Site-Binding Molecules

Ying-Ying Zhang [1†], Yong-Chun Ye [2*†], Jisen Zhang [3†], Bing-Hao Lv [1†], Liu-Jiang Zhang [4], Bi-Yun Shi [1], Qiao-Jun Cao [1], Qiu-Feng Ye [1], Xingyu Gao [4], Haipeng Xie [5], Tingting Shi [3*], Wei-Dong Dou [1*]

[1] Department of Physics, Shaoxing University, Shaoxing, Zhejiang, 312000, China

[2] College of Materials and Chemistry, China Jiliang University Hangzhou, Zhejiang, 310018, China

[3] Siyuan Laboratory, Guangzhou Key Laboratory of Vacuum Coating Technologies and New Energy Materials, Department of Physics, College of Physics & Optoelectronic Engineering, Jinan University, Guangzhou, 510632, China

[4] Shanghai Synchrotron Radiation Facility (SSRF), Shanghai Advanced Research Institute, Chinese Academy of Sciences, Shanghai 201204, China

[5] Institute of Super-microstructure and Ultrafast Process in Advanced Materials (ISUPAM), School of Physics, Central South University, Changsha, Hunan 410083, China

[†] These authors contributed equally to this work.
*Corresponding authors
e-mail: phyth@usx.edu.cn; yongchunye@cjlu.edu.cn; ttshi@jnu.edu.cn

Experimental Section

Materials:

Formamidinium Iodide (FAI), Methylammonium chloride (MACl), Methylammonium bromide (MABr), Lead iodide (PbI_2), Lead bromide ($PbBr_2$), Cesium iodide (CsI), Phenethylammonium iodide (PEAI), [4-(3,6-Dimethyl-9H-carbazol-9-yl)butyl]phosphonic acid (Me-4PACz), and Bathocuproine (BCP) were produced from Xi'an Yuri Solar Co., Ltd. ethyl (methylthio)acetate (EMA, ≥98%) were produced from Shanghai Aladdin Biochemical Technology Co., Ltd. Chlorobenzene (CB, anhydrous, 99.8%), dimethyl- formamide (DMF, anhydrous, 99.8%), Isopropanol (IPA), and dimethyl sulfoxide (DMSO, anhydrous, ≥99.9%) were purchased from Sigma-Aldrich. Indium tin oxide (ITO) coated glass substrates, [6, 6]-Phenyl-C61-butyric acid methyl ester ($PC_{61}BM$), and NiO_x nanoparticle powder were purchased from Advanced Election Technology Company in China. All the materials were used as received without any purification.

Device Fabrication:

ITO substrates were sequentially washed by detergent, ethanol, deionized (DI) water, acetone, and ethanol for 30 min through sonication method, respectively. Cleaned ITO substrates were treated with ultraviolet-ozone for 20 min before use to remove surface impurities and improve wettability. Afterwards, the NiO_x (20 mg mL^{-1} in deionized water) was spin-coated on ITO with 4000 rpm for 30 s and annealed in air (50±5% RH) at 150 °C for 10 min. After cooling down, the substrate was moved to glove box filled with N_2. Then, a thin layer of Me-4PACz (0.3 mg mL^{-1} in IPA) was deposited on NiO_x with 5000 rpm for 30 s and annealed at 100 °C for 10 min. Afterwards, 50 μL of different concentrations of EMA (in IPA)

solutions were spin-coated on substrates at 5000 rpm for 30 s and then the substrates were annealed at 100 °C for 10 min. The perovskite precursor solution was prepared with 1.32 mmol FAI, 0.07 mmol MABr, 0.225 mmol MACl 0.075 mmol CsI, 1.467 mmol PbI_2, and 0.075 mmol $PbBr_2$ in 1 mL mixed DMF and DMSO solvent (volume ratio 4:1). The perovskite precursor solution was spin-coated onto NiO_x film with a two-step program at 1000 and 5000 rpm for 10 and 30 s, respectively, in a nitrogen-filled glovebox. At the last 10th second, a 150 μL anti-solvent of CB was quickly drop-coated, and then the films were annealed at 100 °C for 30 min. After cooling down, PEAI solution (1 mg mL^{-1} in IPA) was spin-coated on the films at 5000 rpm for 30 s, annealed at 100 °C for 5 min. The $PC_{61}BM$ solution (20 mg mL^{-1} in anhydrous CB) was spin-coated on the top of perovskite with 2500 rpm for 40 s. Subsequently, the BCP (0.5 mg mL^{-1} in IPA) was spin-coated with 5000 rpm for 30 s on $PC_{61}BM$ film. Lastly, to finish the solar cell devices, Ag metal electrodes with a thickness of 100 nm were vacuum-evaporated on the BCP substrate with vacuum of 4×10^{-4} Torr. All solution was filtered with a 0.22 μm nylon filter before use.

Property Characterization:

Scanning electron microscope (SEM) images were used to investigate the surface morphology of film by ZESS sigma300. Atomic force microscope (AFM) images were performed at the ambient temperature (Bruker MULTIMODE-8). Steady-state photoluminescence (PL) spectra and time-resolved PL (TRPL) decays of the perovskite films were measured by a Quantaurus-Tau fluorescence lifetime spectrometer (Hamamatsu Photonics). GIXRD measurements were performed at the BL14B1 beamline of the Shanghai Synchrotron Radiation Facility (SSRF) using an X-ray beam (λ=1.2398 Å). FTIR spectra were recorded by Thermo Fisher Scientific

Nicolet iS20. The author would like to thank Mei-fang Wang from Shiyanjia Lab (www.shiyanjia.com) for the FTIR analysis. X-ray photoelectron spectroscopy (XPS) was characterized by an ultrahigh vacuum photoemission spectroscopy system (Kratos AXIS Ultra DLD). Ultraviolet photoelectron spectroscopy (UPS) was employed to understand the changes in energy bands in different samples using a Thermo Escalab 250Xi instrument employing the He I (21.22 eV) emission line for excitation. The ultraviolet-visible (UV-Vis) spectra was recorded on a SHIMADZU, UV-3600 Plus spectrophotometer in 400-900 nm wavelength range. The EIS analysis and M-S measurements were performed on an electrochemical workstation. 3D reconstruction images were obtained by using PHI nano TOF II Time-of-Flight secondary ion mass spectrometry (TOF-SIMS).

Device Characterization:

The J-V characteristic test system of solar cells from Newport in the United States was used, and a 500 W xenon solar spectrum simulator was used for the light source part, and the light source was calibrated with a standard silicon solar cell KG-5 for testing, and the test was carried out at a solar intensity (AM 1.5 G:100 mW/cm^2). Typically, the single-junction devices were measured in reverse scan (1.40 V → -0.1 V) with a scanning speed of 100 mV/s. The output current of the cells is measured by applying a continuously varying voltage (-0.1 V-1.4 V) to both ends of the battery (Keithley 2400 was used as a test power supply). The external quantum efficiency spectrum was measured by NEWPORT 66984-300XF-R1.

Device stability tests:

The thermal stability test following the ISOS-D-2 protocol was conducted in the dark and a nitrogen atmosphere with continuously heating the unencapsulated device at ~60 °C. The

storage stability test following the ISOS-D-1 protocol was conducted in the dark and a nitrogen atmosphere at room temperature.

N_t calculation:

The SCLC curves were based on the electron-only devices (ITO/NiO_x/SAMs/perovskite/spiro-OMeTAD/Ag). The trap density (N_t) is determined by the trap-filled limit voltage (V_{TFL}) based on the following equation:

$$N_t = \frac{2\varepsilon_0\varepsilon_r V_{TFL}}{qL^2}$$

Where L is the thickness of the perovskite film, V_{TFL} is the onset voltage of the trap-filled limit region, ε_r is the relative dielectric constant of perovskite film, ε_0 is the vacuum permittivity, and q is the electron charge.

Ideality factor calculation:

The V_{OC} of PSCs is measured under a range of light intensities (Plight) and plotted as a function of Plight in logarithm scales, and the ideality factor (n) is obtained according to the following formula:

$$V_{oc} = n\frac{kT}{q}\ln I + c$$

where q, K, I, and T are the charge of an electron, the Boltzmann constant, light intensity, and the temperature, respectively.

DFT **calculation:**

First-principles calculations were carried out using the Vienna Ab-initio Simulation Package (VASP), employing the projector augmented wave (PAW) method. The Perdew–Burke–Ernzerhof (PBE) functional within the generalized gradient approximation (GGA) was adopted to describe electron exchange and correlation effects. For the calculations of adsorption energy

and defect passivation, a plane-wave cutoff energy of 400 eV was employed, with energy and force convergence criteria set to 1×10^{-4} eV and 0.05 eV $Å^{-1}$, respectively.

The $FAPbI_3$ (100) surface was constructed with a 3 × 2 × 2 supercell and a Γ-centered 2 × 2 × 1 Monkhorst–Pack k-point mesh. The van der Waals interactions were accounted for using the Grimme DFT-D3 with the zero-damping function in adsorption energy calculations. Additionally, the electrostatic potential (ESP) of EMA was computed using all-electron double-ζ valence basis sets. All crystal structures were constructed using Materials Studio and visualized with VESTA.

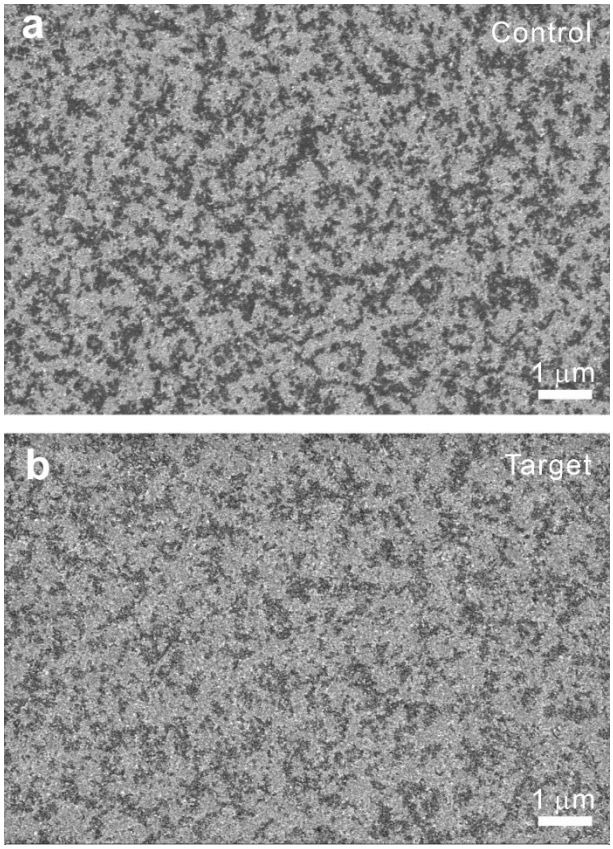

Figure S1. SEM images of NiO_x films without a) and with b) EMA modification.

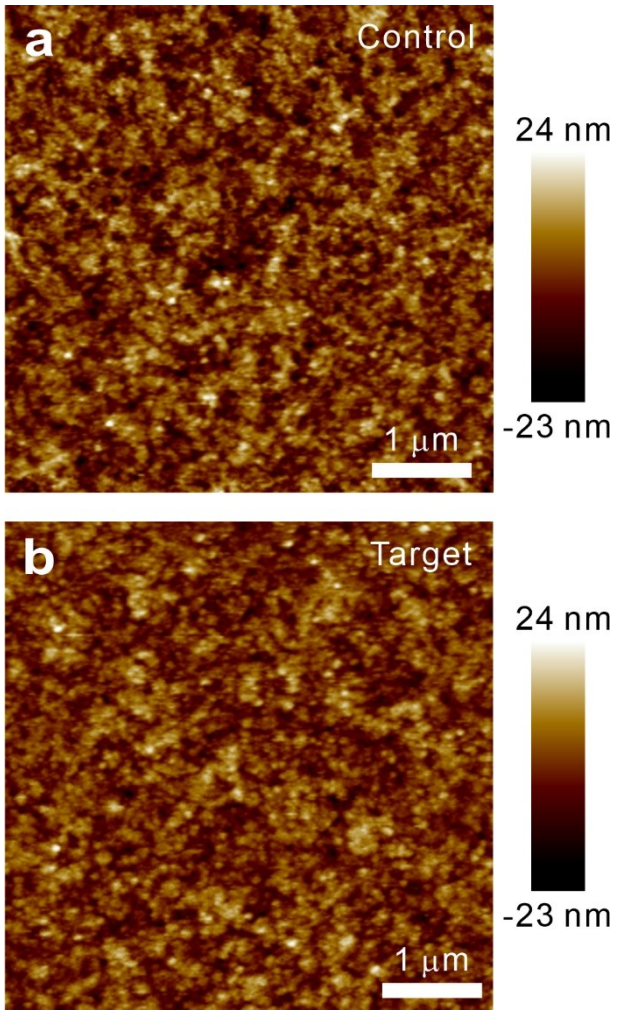

Figure S2. AFM images of NiO_x films without a) and with b) EMA modification.

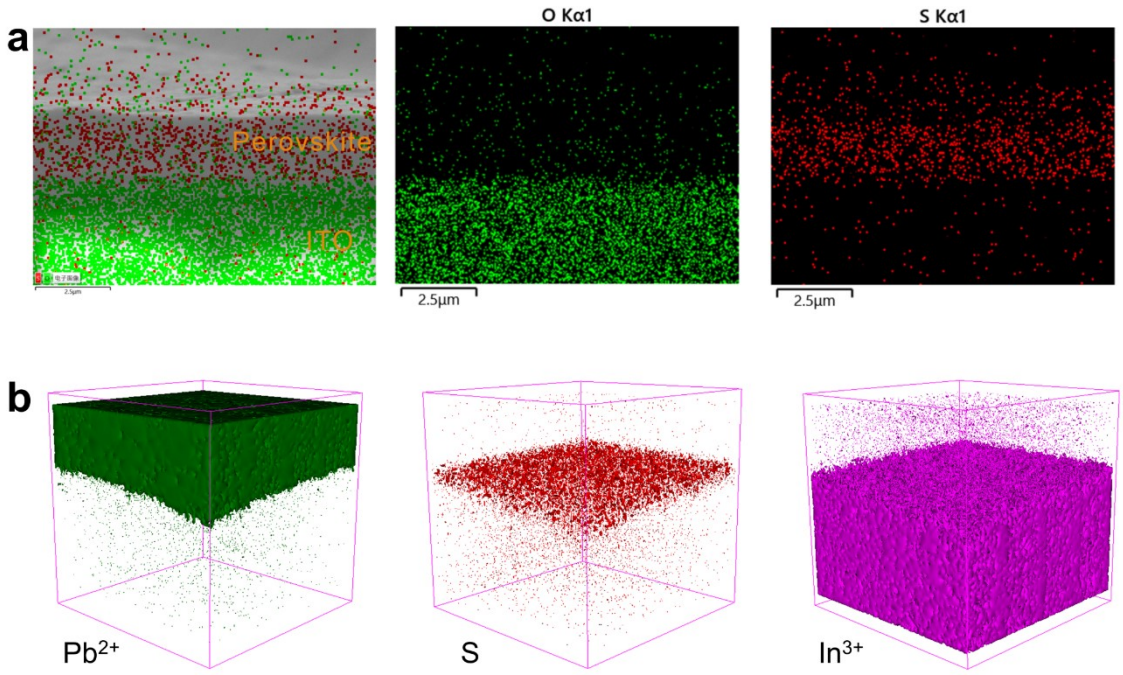

Figure S3. (a) High-magnification cross-sectional SEM images of EMA-modified perovskite film. (b) ToF-SIMS depth profiles of the EMA-modified perovskite film.

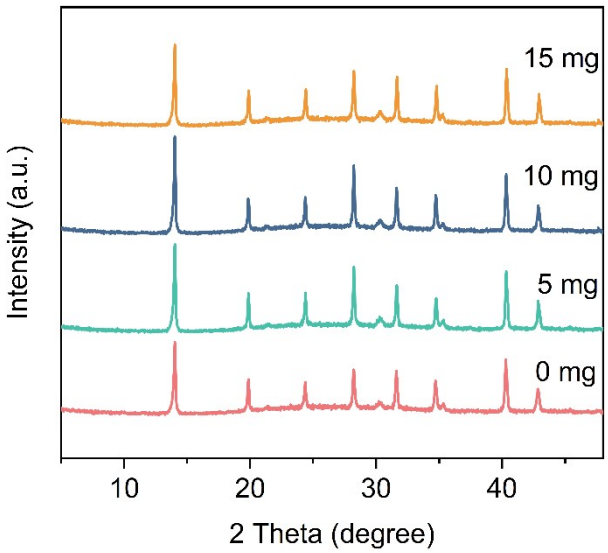

Figure S4. XRD patterns of perovskite thin films treated with different amount of EMA.

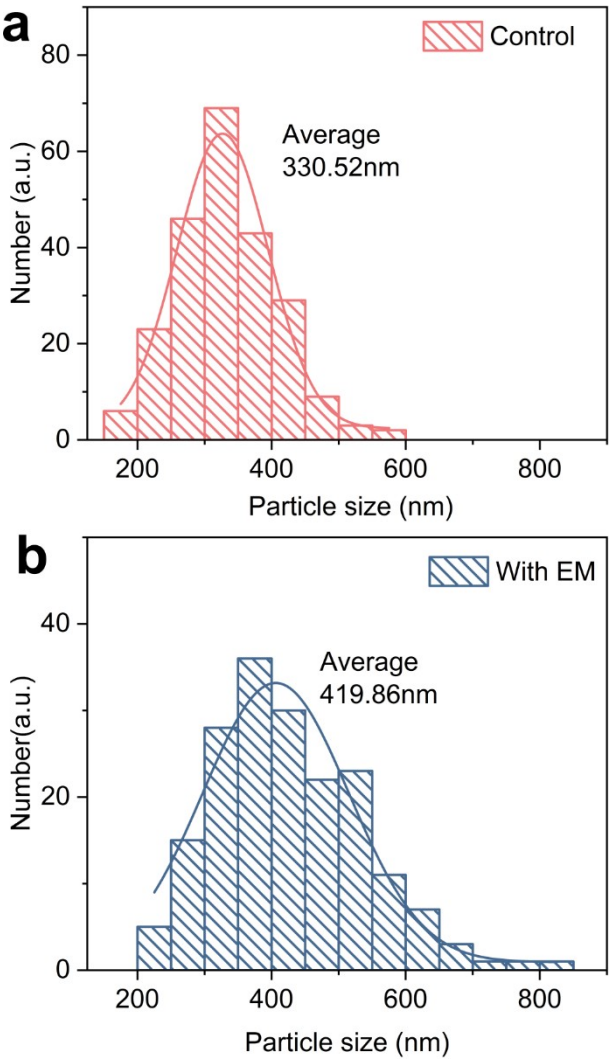

Figure S5. The grain size distributions of the perovskite film deposited on NiO_x/Me-4PACz a) and NiO_x/Me-4PACz/EMA b) substrates.

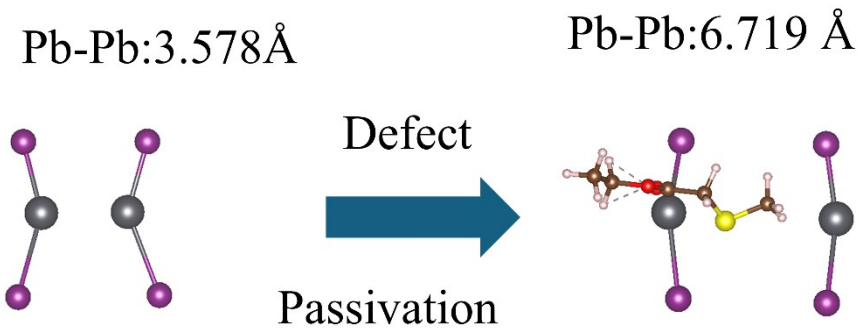

Figure S6. Schematic diagram of the Pb-dimer structure before and after defect passivation.

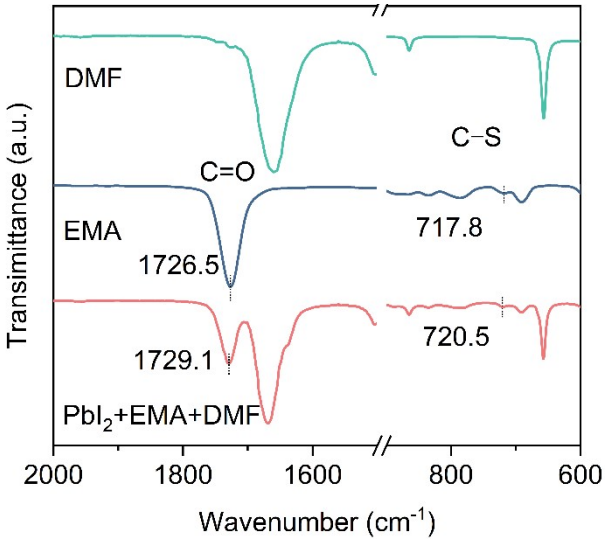

Figure S7. FTIR spectra for DMF, PbI_2 and PbI_2+EMA.

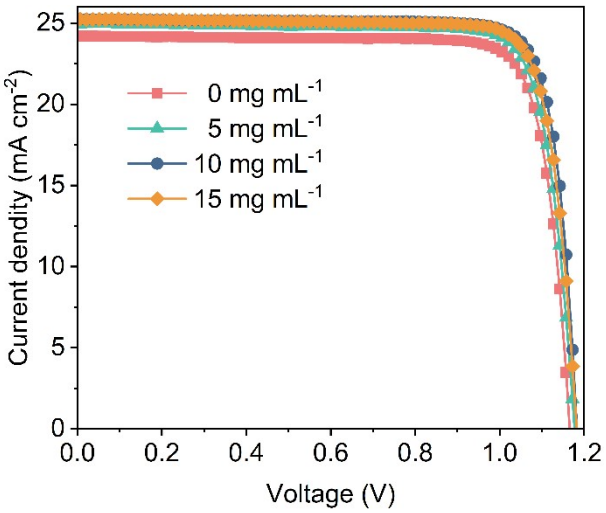

Figure S8. *J–V* curves of PSCs modified with different EMA concentrations.

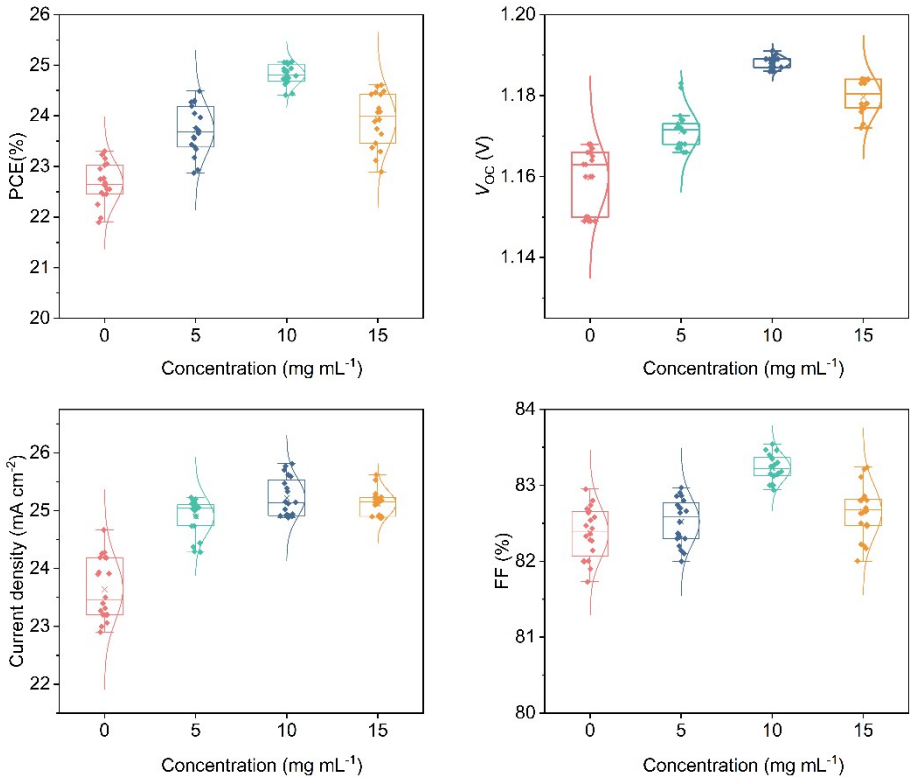

Figure S9. Distribution of PCE, V_{OC}, J_{sc}, and *FF* parameters in *J–V* characterization treated with different amount of EMA.

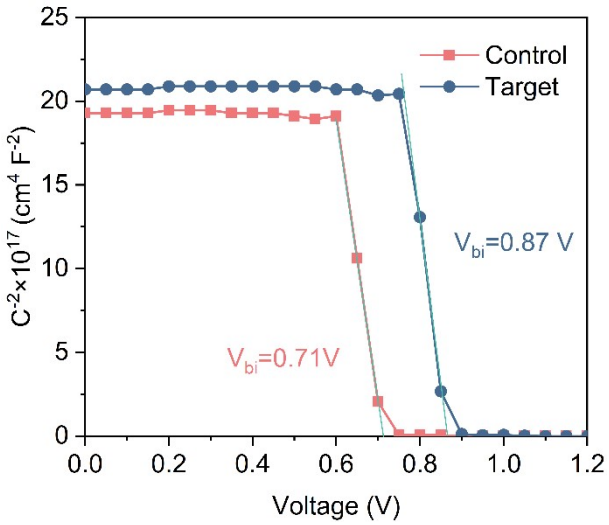

Figure S10. Mott−Schottky plots of the device without and with EMA modification.

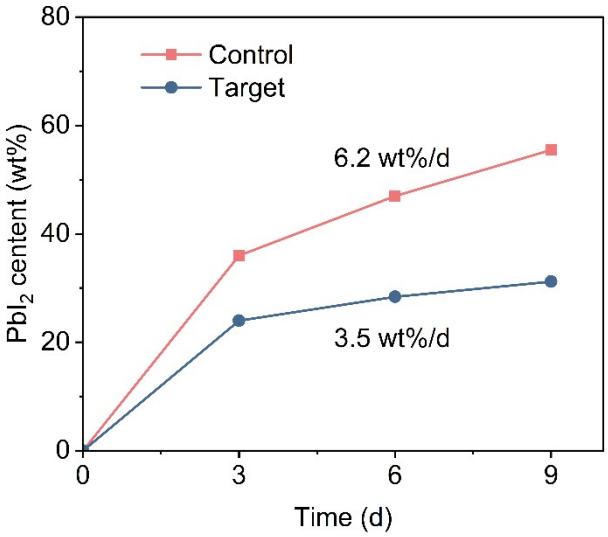

Figure S11. The content of PbI_2 in perovskite films.

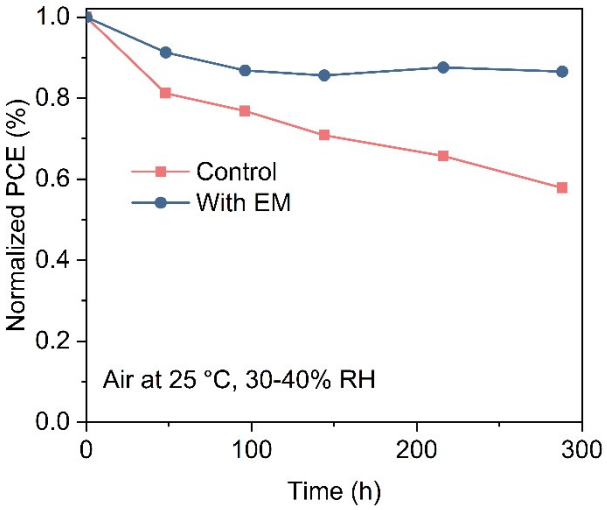

Figure S12. Stability test of unencapsulated devices in air atmosphere.

Table S1. Summary of photovoltaic PCE and number of binding sites of reported NiO_x-based inverted PSCs in recent years.

Device structures	Year	Number of binding sites	PCE (%)	Ref.
ITO/NiO_x/Me-4PACz/perovskite/PI/PCBM/BCP/Bi/Ag	2024	3	26.54*	[1]
ITO/NiOx/SAMs/perovskite/PEAI/PCBM/BCP/Ag	2024	1	25.4	[2]
ITO/NiO_x/Me-4PACz/perovskite/PCBM+C_{60}/BCP/Ag	2024	1	25.09	[3]
ITO/NiO_x/MeO-4PACz/ADAI/perovskite/C_{60}/BCP/Ag	2025	1	25.36*	[4]
ITO/NiO_x/3F-PTES/perovskite/C_{60}/BCP/Ag	2025	3	26.47	[5]
FTO/ALD-NiO_x/3PATAT/perovskite/C_{60}/BCP/Ag	2025	3	25.1	[6]
FTO/NiO_x/2PACz-3-UA/perovskite/PCBM/BCP/Ag	2025	1	25.3	[7]
FTO/NiOx/BTSA/perovskite/C_{60}/BCP/Ag	2025	2	26.65*	[8]
FTO/NiO_x/SAM/perovskite/PCBM/BCP/Ag	2025	1	26.05	[9]
ITO/NiO_x/Me-4PACz/perovskite/PCBM/BCP/Ag	2026	1	26.62*	[10]
ITO/NiO_x/Por-N-O/perovskite/ C_{60}/BCP/Cu	2026	2	27.05	[11]
ITO/NiO_x/Me-4PACz/perovskite/PCBM/BCP/Ag	2026	2	25.05	This work

*Certified PCE.

Table S2. Time-resolved PL curve fittings of the perovskite films under an excitation pulse at 373 nm.

Samples [/]	PL peak [nm]	τ_1 [ns]	τ_2 [ns]	τ_{avg} [ns]
Control	798	13.5	244.7	167.3
Target	798	12.6	206.1	141.2

Notes: The time-resolved PL decay curves measured by time-correlated single-photon counting were fitted by a bi-exponential equation: $Y=A_1\exp(-t/\tau_1)+A_2\exp(-t/\tau_2)$. Here, A_1 and A_2 correspond to the decay amplitudes of fast and slow components, respectively, where $A_1+A_2=1$. The average lifetime τ_{avg} was calculated by $\tau_{avg}=(A_1\tau_1^2+A_2\tau_2^2)/(A_1\tau_1+A_2\tau_2)$.

[1] S. Liu, J. Li, W. Xiao, R. Chen, Z. Sun, Y. Zhang, X. Lei, S. Hu, M. Kober-Czerny, J. Wang, F. Ren, Q. Zhou, H. Raza, Y. Gao, Y. Ji, S. Li, H. Li, L. Qiu, W. Huang, Y. Zhao, B. Xu, Z. Liu, H. J. Snaith, N.-G. Park, W. Chen, *Nature* **2024**, *632*, 536.

[2] S. Cao, S. Luo, T. Zheng, Z. Bi, J. Mo, L. G. Gutsev, N. A. Emelianov, V. V. Ozerova, N. A. Slesarenko, G. L. Gutsev, S. M. Aldoshin, F. Sun, Y. Tian, B. R. Ramachandran, P. A. Troshin, X. Xu, *Adv. Energy Mater.* **2025**, *15*, 2405367.

[3] Q. Cao, T. Wang, X. Pu, X. He, M. Xiao, H. Chen, L. Zhuang, Q. Wei, H. Loi, P. Guo, B. Kang, G. Feng, J. Zhuang, G. Feng, X. Li, F. Yan, *Adv. Mater.* **2024**, *36*, 2311970.

[4] C. Xu, P. Hang, C. Kan, X. Guo, X. Song, C. Xu, G. You, W.-Q. Liao, H. Zhu, D. Wang, Q. Chen, Z. Hong, R.-G. Xiong, X. Yu, L. Zuo, H. Chen, *Nat. Commun.* **2025**, *16*, 835.

[5] Y. Wang, Y. Feng, H. Yang, S. Li, K. Zhang, Y. Feng, X. Han, T. Alshahrani, Q. An, X. Wang, H. Li, Y. Jiang, M. Yuan, *Adv. Mater.* **2025**, e07730.

[6] Y. Xu, C. Wang, U. Amornkitbamrung, H. J. Jeong, R. J. K. Rhee, Y. In, A. Gibson, T. Nakamura, M. A. Truong, A. Wakamiya, H. Shin, *ACS Energy Lett.* **2025**, *10*, 3407.

[7] Z. Zhang, T. Wu, Z. Qin, M. Chen, W. Xiang, Z. Chen, Y. Wang, Z. Guo, T. Matsushima, L. Han, *Adv. Energy Mater.* **2025**, *15*, 2500572.

[8] J. Ding, Y. Liao, H. Liu, Y. Ding, Q. Ma, M. Li, Z. Zhang, J. Zhang, J.-X. Tang, J. Sheng, J. Chen, C. Chen, *Nat. Commun.* **2025**, *16*, 8407.

[9] F. Song, N. Yan, Y. Cao, J. Zhang, D. Qi, J. Shan, Y. Liu, L. Jiang, T. Li, L. Li, S. (Frank) Liu, J. Feng, *Angew. Chem. Int. Ed.* **2025**, *64*, e202516012.

[10] K. Li, Z. Zhang, S. Sun, S. Dong, X. Lu, Y. Liu, M. Dai, L. Li, F. Li, Z. Li, H. Zhang, Y. Zhai, S. Li, H. Wang, X. Zhu, C. Chen, J. Chen, T. Zhu, *Adv. Mater.* **2026**, *38*, e72638.

[11] C. Chen, C. Lu, Z. Suo, X. Mu, Y. Yang, J. Cao, *Adv. Mater.* **2026**, *38*, e21697.